Diagnostic Tools for Lithium-ion Batteries

Catarina Matias Vieira, Prof. João Salvador Fernandes[1]

1- Supervisor, Instituto Superior Técnico, Universidade de Lisboa.

November 2022

Abstract

One of the main difficulties associated with the management of end-of-life electric vehicle batteries is related to the diagnosis of their state of health (SOH). This diagnosis is fundamental to evaluate the battery's state compared to its initial state, and thus making a decision regarding its possible use in second life applications.

The goal of this work is to understand the degradation phenomena of lithium-ion batteries by applying the Electrochemical Impedance Spectroscopy technique over charge-discharge cycles, with subsequent analysis through an Electrical Equivalent Circuit.

Determining the SOH of a battery based on capacity loss requires applying a full charge and discharge, and this process is quite time consuming and impractical. Alternatively, the SOH can be calculated based on the internal resistance of the cell.

A new cell, a cell already used in an electric vehicle, two new cells connected in parallel and two used cells connected in parallel were tested over 50 charge-discharge cycles. Through analysis of the impedance spectra and the Electrical Equivalent Circuit it was found that the internal resistance is the parameter that contributes most to the total impedance of the cell and that the variation of the internal resistance may be used as an indicator of the evolution of the capacity.

Different methods for determining SOH based on impedance and internal resistance were presented and tested in order to seek a correlation with the SOH values calculated using capacity.

Keywords: Lithium-ion Batteries, State-of-Health, Electrochemical Impedance Spectroscopy, Charge-Discharge cycles, Electrical Equivalent Circuit.

1. Introduction

Given the increasing growth in global energy consumption and the reliance on fossil fuels as the energy source, it is urgent to find alternatives for more sustainable and cleaner energy production, greenhouse gas (GHG) emissions reduction and more efficient energy storage[1,2]. Energy storage through batteries becomes advantageous as those are compact and portable devices. In the transportation sector, the demand for Electric Vehicle (EV) batteries has been growing fast, increasing from about 40 to 155 GW/year between 2015 and 2020, with a particularly significant growth for light-duty vehicles[3]. Due to its electric motor, these vehicles emit less or no GHG while in use, unlike internal combustion engine vehicles (ICEVs), showing great potential for reducing global GHG emissions.

Despite the advances that have been made in the electric mobility sector, the useful lifetime of batteries used in EVs is still a major limitation. As a result of various ageing mechanisms that occur during the life cycle of a battery, it degrades over time, resulting in capacity and power fade. Understanding these ageing mechanisms is of utmost importance for battery state estimation.

The challenge relies on simple, cost-effective, and fast monitoring and diagnosis of battery condition during and after its use in an EV, which allows not only to understand when it should be replaced, but also to decide according to its condition whether it still fits the requirements for a second life application. Among the established indicators that characterize the state of a battery, SOH shows to be extremely useful in the evaluation of Li-ion batteries used in EVs, since SOH assesses the condition of a battery compared to its initial state and quantitatively evaluates the battery's remaining usable capacity. However, capacity measurement involves a complete charge and discharge, which is time and energy-consuming, especially if an analysis is performed on battery modules rather than individual cells. Given that resistance increase is critical for the performance of EV batteries, it should be evaluated and considered for battery state assessment.

2. Literature Review

Some of the characteristics that make LIBs so attractive for energy storage applications, in particular as traction batteries for EVs and PHEVs are lithium's small ionic radius, which facilitates its diffusion, and its low molecular weight that allows

for lighter-weight batteries and devices. Additionally, lithium is the metal with the lowest reduction potential value ($E°(Li^+/Li)$ =-3.04V vs standard hydrogen electrode), resulting in a higher energy density[4,5]. LIBs outperform other types of secondary batteries in terms of specific energy (can reach up to 450Wh/kg in the case of $LiCoO_2$/graphite cells), and lifetime (lasting over 20000 cycles in $Li_4Ti_5O_{12}$ negative electrode cells)[6]. Additionally, LIBs can reach power density values up to 3000W/kg in the case of $LiFePO_4$ (LFP)/graphite cells [7]. There are different types of LIBs that differ essentially in the composition of the positive electrode, which is a transition metal oxide. For the anode, lithium-titanate ($Li_4Ti_5O_{12}$) or different forms of carbon compounds may be used, graphite being the most widely used material[2,8].

When a LIB is charging, the Li-ions flow from the cathode and are intercalated in the anode and, at the same time, the electrons are attracted to the current collector and move from the cathode to the anode through the external current circuit. At the anode, the Li-ions are accommodated in the graphite structure[8–10]. During the discharge of the battery, the process is the opposite: the lithium is oxidized to Li^+ at the anode and Li-ions migrate to the cathode through the separator, being reduced to Li at the cathode and intercalated in the cathode structure. The movement of Li-ions from the anode to the cathode forces the electrons to flow through the electric circuit, generating the electric current that powers a device[9].

During the first cycles of a battery, the Solid Electrolyte Interphase (SEI) forms between the anode and the electrolyte due to the reduction of the electrolyte. Its formation is extremely important as it prevents electron tunnelling, reduces the kinetics of electrolyte decomposition and decreases the lithium consumption [11,12].

There are complex mechanisms involved in the ageing of LIBs, which can be, according to Pastor Fernández et al.[13] , divided into three Degradation Modes (DMs): conductivity loss (CL), loss of active material (LAM), and loss of Li inventory (LLI). CL is related to the degradation of the electronic parts of the battery and includes corrosion of current collectors and binder decomposition. LAM is related to structural transformations in the active material, including particle cracking, electrolyte oxidation, electrode decomposition, and structure disorder. LLI is related to the decline in the number of Li-ions available for intercalation and deintercalation reactions by being consumed in parasitic and decomposition reactions, including SEI growth and decomposition, electrolyte decomposition, and lithium plating [7,13,14].

The ageing of LIBs can be caused by both intrinsic and extrinsic factors. Defects related to the methods and materials used in the fabrication are examples of intrinsic factors that can affect ageing. Extrinsic factors are related to the operating conditions applied to the battery, such as temperature, charge and discharge rates, depth of discharge (DOD), and state-of-charge (SOC)[14]. In addition to the influence that each of these factors has on the ageing of a single cell, a battery can be subjected to inhomogeneous conditions, such as having cells operating at different temperatures and non-uniformly distributed currents[7,9,13.]

Temperatures above 35ºC promote electrolyte decomposition and SEI growth, while below 5ºC lithium platting, dendrite formation and electrolyte decomposition by the metallic lithium can occur. Applied currents higher than 2C can lead to volume changes and gas generation, with consequent particle cracking and SEI growth. A SOC higher than 95% enhances electrolyte and binder decomposition, gas generation and crack formation, while overdischarging the battery leads to corrosion of the current collectors and binder, and structural disorder. A DOD higher than 70% leads to volume changes and consequent particle cracking[13]. As a result of these ageing processes, the internal resistance of the battery increases (power fade), and the capacity decreases (capacity fade), which in the case of EVs translates into a reduction of the driving range and power of the vehicle, respectively [9,13]. Capacity loss of LIBs is mostly attributed to the SEI, initially with its formation and growth, and later due to SEI formation in graphite exposed to the electrolyte due to fractures[15,16]. LIBs are characterized by three main stages of degradation: 1) rapid capacity fade associated with initial SEI formation; 2) approximately linear ageing in terms of capacity associated with lithium consumption in secondary reactions; 3) rapid capacity fade as the cell approaches the end of its life until it eventually fails, associated with an impedance rise [17].

Regarding EV batteries, the capacity and internal resistance are extremely important parameters for battery condition assessment, since these are what the replacement criteria are based on. The experimentally obtained parameters can then be translated into battery state indicators, such as State-of-Charge (SOC), State-of-Energy (SOE), State-of-Power (SOP), State-of-Temperature (SOT), State-of-Safety (SOS), and State-of-Health (SOH)[7]. The SOH is an indicator that quantitatively assesses the state of a battery compared to its initial one in terms of

storage and release of electrical energy[18,19]. Battery ageing in terms of capacity can be calculated as follows:

$$SOH = \frac{C_a}{C_r} \times 100\% \quad (1)$$

, where C_a and C_r represent the actual and rated capacity values, respectively[18]. This definition is not consensual among authors. For example, in the definition proposed by Hu et al.[18], a SOH of 0% is reached only when the battery's capacity C_a equals zero. According to this definition, a battery should be replaced at a SOH of 80%. On the other hand, authors such as Ungurean et al.[20] defend that the moment when the battery is replaced, i.e., when the capacity reaches 80%, corresponds to a SOH of 0%. In this work, SOH based on capacity is defined as in [18], assuming battery replacement at SOH of 80%.

Another alternative is to define SOH based on the battery's internal resistance, as follows:

$$SOH = \frac{R_{int,subs} - R_{int}}{R_{int,subs} - R_{int,NEW}} \times 100\% \quad (2)$$

, being $R_{int,subs}$ the internal resistance when the battery is substituted, R_{int} is the current internal resistance and $R_{int,NEW}$ is the internal resistance of the battery as new[20].

However, this definition is also not as straightforward. First, because at the moment when the battery is replaced, the SOH would be 80% for the capacity-based SOH definition, while it would be 0% using the resistance-based SOH definition. Furthermore, $R_{int,NEW}$ is not always readily available for all cell models.

3. Methodology

To fully understand the processes occurring in a cell as it ages, Electrochemical Impedance Spectroscopy (EIS) was the selected technique, as it provides important information on the electrochemical dynamics of a cell. EIS can be combined with cycling tests, where the capacity is measured, by being performed at different charge states, after a charge or discharge step.

3.1. Charge-discharge cycles

The measurement of cell capacity can be done during a full charge or discharge by Coulomb counting. LIBs are typically charged using the Constant Current - Constant Voltage (CC-CV) mode. The main disadvantage of cycling tests is their duration. The specified charge and discharge currents cannot be too high to avoid excessive ageing, which coincides to long testing times. Furthermore, the CV stage during charging takes longer than the CC stage, meaning that even after reaching the maximum potential, the battery continues charging for an even longer timeframe. In the viewpoint of EV batteries, if capacity testing is performed to a stack of cells connected in series and/or in parallel, the total testing time increases substantially, demanding that the vehicle cannot be used for several hours.

3.2. Electrochemical Impedance Spectroscopy

EIS followed by Electrical Equivalent Circuit (EEC) analysis not only provides important information on the electrochemical dynamics of a cell, but it is also the only technique where the different contributions to the total impedance can be separately identified, allowing analyzing the resistive component of impedance[14].

Impedance values are usually measured over a frequency range between 100 kHz and 10 mHz[21]. A Nyquist plot can be divided into different frequency regions, each of them related to certain dynamics and electrical behavior. The Z_{real} value when the Nyquist plot intersects the X-axis at high frequencies represents a purely resistive behavior: the internal resistance of the cell. In the middle frequency region, the first semicircle is attributed to the SEI, while the second relates to the charge transfer process, both having a capacitive and a resistive component. In the low frequency region, the 45º slope line represents the Warburg impedance, which is related to the diffusion process [13,22].

It is possible to distinguish and quantify different resistances in the real axis of a Nyquist diagram of a battery, namely, the internal resistance of the cell (R_{int}), of the Solid Electrolyte Interphase (R_{SEI}), of the charge transfer reaction (R_{CT}), and of the diffusion process (W) (Figure 1).

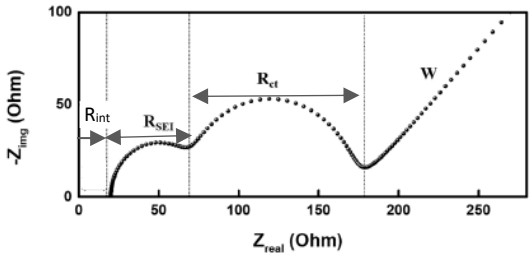

Figure 1: R_{int}, R_{SEI} and R_{CT} on a Nyquist plot.

It is common to analyze the impedance of a battery by fitting it to an EEC. The choice of an EEC should be focused not only on a good fitting result but mostly on its physical meaning, i.e., the model should be directly related to the physical processes occurring in the cell. The preferred model for LIBs whose Nyquist diagram shows two semicircles is composed of a resistor to represent the internal resistance, a ZARC circuit to represent the first semicircle, and, to represent the second semicircle and the diffusion process, a

ZARC circuit is used, where in the resistor branch a Warburg element is added in series, as the charge transfer is limited by diffusion[14,21]. This model is represented in Figure 2.

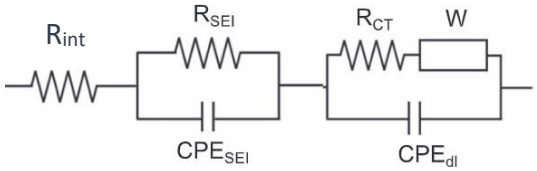

Figure 2: Simplified electrical equivalent circuit for a lithium-ion battery.

, where R_{int} represents the internal resistance of the cell (which includes the resistances of the electrolyte, separator and current collectors); R_{SEI} and CPE_{SEI} represent the resistance and capacitance of the SEI, respectively; R_{CT} represents the charge transfer resistance in the cathode; CPE_{dl} represents the capacitance of the double layer at the cathode and W represents the mass transport [21,23].

As the battery degrades, the Nyquist diagram shifts to higher Z_{real} values, and some changes in the shape of the semicircles are observed[7,21]. R_{int} is not expected to present any significative changes with SOC. Instead, R_{int} increases with the number of cycles, mostly due to electrolyte decomposition and SEI formation from its decomposition products. Since these are the most significant ageing mechanisms in LIBs, R_{int}, is normally the parameter that changes more substantially with cycling, thus R_{int} is a very important parameter on the determination of the SOH of a battery. However, it is noteworthy that the first semicircle of the Nyquist plot is related to the SEI, so the contribution of SEI formation to R_{int} increase consists only in being a secondary effect of electrolyte decomposition[13,14,21,22]. The SEI is a solid layer that forms at the interface between the anode and the electrolyte, thus having both capacitive and resistive properties, represented in a Nyquist diagram by a semicircle. SEI formation and growth makes the intercalation and de-intercalation reactions of Li-ions more difficult by acting as a barrier to their movement, causing simultaneously an impedance increase and a loss of capacity. Since this growth happens gradually over time, R_{SEI} is expected to increase with the number of cycles [13,23]. The second semicircle is related to the interfacial processes, comprising the reactional impedance, R_{CT}, and the double layer capacitance. A fully charged battery has a high R_{CT}, because during charging the Li-ions moved to the anode, occupying a large portion of the intercalation spaces. As there are fewer intercalation spaces at the anode to accommodate Li-ions, the resistance to transfer of ions and electrons increases. When the battery starts to be discharged, the reaction occurs in the opposite direction. Thus, Li-ions migrate to the still lithium-poor cathode, so R_{CT} decreases dramatically at this early stage of discharge since there are still many free intercalation spaces and both ions and electrons flow easily. As the discharge proceeds, R_{CT} increases, reaching its maximum when the battery is fully discharged. Overall, R_{CT} values are higher for a completely discharged battery than for a completely charged one, which is attributed to the structure of the cathode itself, which offers more resistance to Li-ion transfer than the graphite. Furthermore, R_{CT} is expected to increase with cycling since both Li-ions and electrons take part in secondary irreversible reactions, such as SEI formation and growth. Thus, the SEI is only indirectly related to R_{CT} since it is a solid barrier that hinders charge transfer and its formation and growth consume active material[13,23]. Warburg impedance is always higher for lower frequencies, given that the distance over which species diffuse is greater.

4. Experimental Part

In this work, two types of cells were studied: 1) Panasonic NCR18650B cells, 3.6V nominal voltage, NCR cathode, 3.25Ah capacity. These commercial cells were acquired as new; 2) Panasonic NCR18650 cells, 3.6V nominal voltage, NCR cathode, 2.9Ah capacity. These cells are inserted in a discarded battery module of an electric. For simplicity, these cells are further designated as “new cells” and “used cells”, respectively. One cell of each model was subjected to 50 charge-discharge cycles. The applied currents are the specified ones for each model. CC-CV charge was done, and the discharge was divided into four steps of equal potential intervals. After each charge and discharge step impedance was measured by galvanostatic EIS after a rest period (1 hour after charging and 30 minutes after each discharge step). Afterwards, two new cells were connected in parallel and subjected to 50 charge discharge cycles, as well as two used cells connected in parallel. Every 5 cycles the discharge was done in 4 steps (“long cycle”), like it was done for the individual cells, and for the rest of the cycles the discharge was done in one step only (“fast cycle”), with EIS measurement after the complete charge and the complete discharge.

5. Results and discussion

The EEC defined for the studied batteries is shown in Figure 2 and it revealed to be a good physical approximation to the processes happening in the cell, with the addition of having a goodness of fit in the order of 10^{-6}.

5.1. Capacity and impedance analysis of individual cells

New cell

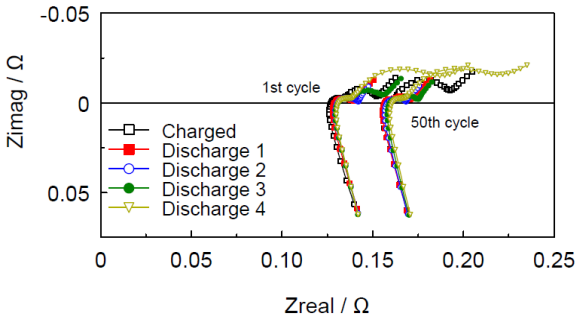

Figure 3: Nyquist plots of a new cell at different charge states for the 1st and 50th cycles.

For both the 1st and 50th cycles of the new cell, R_{int} increases slightly as the cell is being discharged. While R_{SEI} does not show significant variation, R_{CT} decreases significantly at the beginning of the discharge, increasing gradually for lower SOC. Likewise, W_o increases as SOC decreases, as diffusion gets gradually more difficult. It is clear that R_{int} is the parameter which changes the most from the first to the last cycle, by increasing 23.9%.

The Nyquist plots of the totally charged cell revealed that R_{CT} evolves irregularly over cycling, increasing and decreasing over the 50 cycles, and that more unstable variations of R_{CT} correspond to more irregular variations in capacity, even though their evolution does not seem to be related. This irregular R_{CT} variation suggests that the resistance of a cell does not necessarily increase over consecutive cycles, i.e., impedance rise with ageing is verified, but it is not linear. R_{SEI} decreased slightly, which was attributed to the fact that in a new cell the SEI layer is not yet stable during the first cycles, and once it stabilizes R_{SEI} is expected to increase. W_o increased gradually with cycling.

Used cell

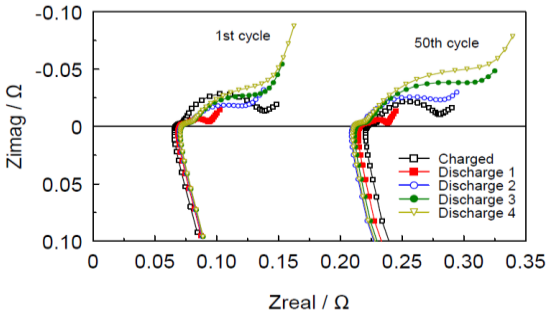

Figure 4: Nyquist plots of a used cell at different charge states for the 1st and 50th cycles.

In the used cell, a small increase on R_{int} as SOC decreases was verified in the 1st cycle, but not in the 50th. There were no substantial changes in R_{SEI}, and R_{CT} showed the same behavior as for the new cell. W_o increases as SOC decreases, except after the last discharge state, where is decreases. R_{int} is the parameter that changes the most, increasing 237.8%. However, this increase was found not to be gradual. R_{int} decreased between the 30th and the 38th cycles, which coincided with a capacity gain. In addition, a significant increase in R_{int} was found between the 24th and 28th cycles, coinciding with a large capacity drop. This finding suggests a possible relationship between capacity and internal resistance.

R_{SEI} did not show any significant changes over cycling, while R_{CT} varied irregularly, and W_o slightly decreases. The variation of R_{CT} did not show any correlation with capacity variation and a decrease in W_o was attributed to particle cracking due to more extensive ageing, which affects the Li diffusion path.

5.2. Capacity and impedance analysis of two parallel-connected new cells

New cells

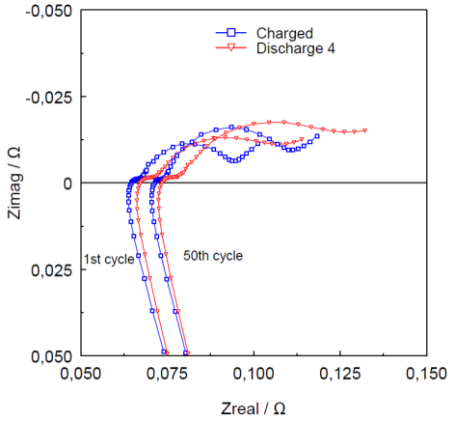

Figure 5: Nyquist plots of two new cells connected in parallel at the charged and discharged states for the 1st and 50th cycles.

Both the 1st and 50th cycles show a similar behavior. R_{int} increases slightly as SOC

decreases and R_{SEI} does not show considerable changes. R_{CT}, decreases strongly from the charged state to the first discharge, and increases gradually as the discharge progresses. Warburg impedance increases for lower SOC. R_{int} increased 10% over the 50 cycles. R_{CT} and W_o also increased over cycling, even though there were found some decreases.

Used cells

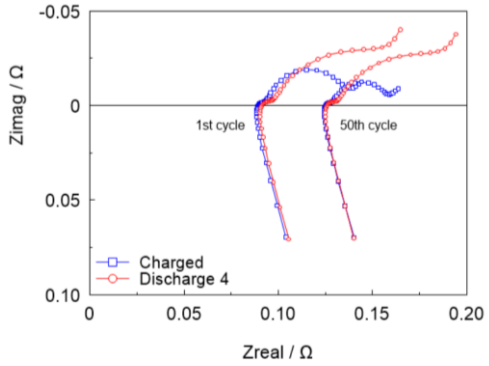

Figure 6: Nyquist plots of two used cells connected in parallel at the charged and discharged states for the 1st and 50th cycles.

The impedance of two used cells in parallel over a single cycle follows the same evolution as individual used cells. R_{int} is again the parameter which changes the most, increasing 39.4%. A clear decrease of the second semicircle is also noted.

Capacity varies more irregularly than R_{int} but with a decreasing tendency, increasing only in the last 4 cycles, which coincides with the overall increase in R_{int}, except for the last cycles, when it decreases. R_{SEI} does not present any substantial variation during cycling and R_{CT} is the highest in the 1st cycle, showing an irregular variation from the 10th cycle onwards. W_o shows a small decrease over the 50 cycles. R_{CT} and W_o show to vary much more with SOC than with cycling.

5.3. SOH definition based on impedance

To evaluate the weight of R_{int}, R_{SEI}, and R_{CT} and W_o on the overall impedance, their evolution with cycling was compared to the variation of |Z|. It was found that for all the studies (individual new and used cell and parallel-connected new and used cells), R_{int} is the resistance that contributes the most to |Z|, regardless of the SOC, suggesting that it could be used as an indicator of battery ageing for SOH estimation. Therefore, R_{int} variation over cycling was compared with capacity evolution.

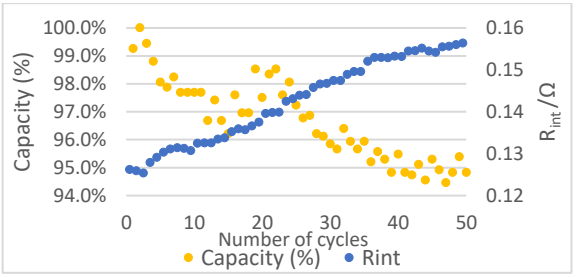

Figure 7: Capacity and R_{int} variation of a new charged cell over cycling.

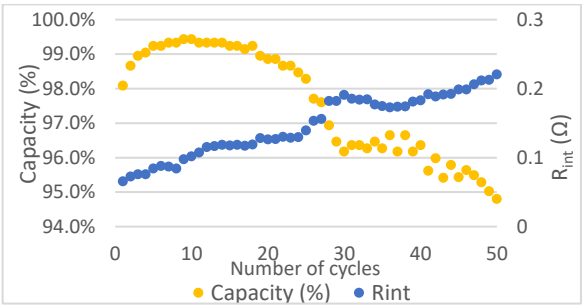

Figure 8: Capacity and R_{int} variation of a used charged cell over cycling.

For the new cell (Fig. 7), capacity has a decreasing tendency, except in between the 15th and the 20th cycles, while R_{int} keeps increasing over the 50 cycles. For the used cell (Fig. 8), except for the first 10 cycles, where both capacity and R_{int} increase, these two parameters show an opposite behaviour, with R_{int} increasing when capacity decreases and vice versa.

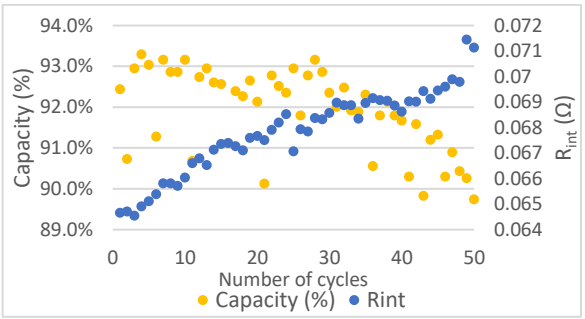

Figure 9: Capacity and R_{int} variation of two new cells connected in parallel with cycling.

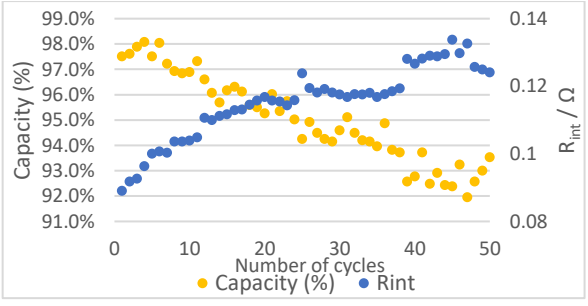

Figure 10: Capacity and R_{int} variation of two used cells connected in parallel with cycling.

In the case of the new parallel-connected cells (Fig. 9), since both capacity and R_{int} vary very irregularly, it is difficult to find a relationship between them.

Overall, the parallel association of used cells (Fig. 10) presents an increase of R_{int} with cycling, accompanied by a decrease in capacity. In the last four cycles, capacity increases while R_{int} decreases.

According to the capacity-based definition of SOH (SOH_C), the moment when the battery in an EV is replaced corresponds to a SOH of 80%, while according to the resistance-based SOH definition, this moment corresponds to a SOH of 0%. Therefore, an alternative resistance-based definition is proposed. Instead of the value $R_{int,subs}$, the internal resistance when the battery is replaced, it is used the value $R_{int,EOL}$, corresponding to the internal resistance of the battery when it dies, i.e. to the end-of-life of the battery, which is the moment when the SOH is considered 0%. SOH is defined as 80% when the battery is replaced. Thus, the challenge is to estimate $R_{int,EOL}$ as a function of $R_{int,NEW}$ to use in SOH calculation.

The estimation of $R_{int,EOL}$ is done based on the resistance-based battery replacement criteria. Since a battery must be replaced when its R_{int} doubles, i.e., when $R_{int} = 2R_{int,NEW}$, and considering that at that moment the SOH is 80%, then $R_{int,EOL}$ can be calculated as follows:

$$SOH = \frac{R_{int,EOL} - 2\,R_{int,NEW}}{R_{int,EOL} - R_{int,NEW}} = 0{,}80$$
$$\Rightarrow R_{int,EOL} = 6\,R_{int,NEW} \quad (3)$$

Therefore, SOH determination based on this criterion, SOH_2, can be calculated as:

$$SOH_2 = \frac{6\,R_{int,NEW} - R_{int}}{6\,R_{int,NEW} - R_{int,NEW}} \times 100\% \quad (4)$$

The advantage of this approach to calculate SOH is that the relationship $R_{int,EOL} = f \cdot R_{int,NEW}$ is fixed for all lithium-ion cell types, meaning that SOH_2 can be easily estimated as long as $R_{int,NEW}$ is specified by the manufacturer.

SOH_C and SOH_2 seem to have a reasonable correlation in the case of the new cell (Fig. 11) and in the case of the association of two used cells in parallel (Fig. 14), suggesting that achieving 80% of the rated capacity may coincide to reaching twice the rated internal resistance, even though 80% of the capacity was not achieved over 50 cycles. In the case of the used cell, these two definitions of SOH do not seem to be related, as capacity decreases much less than internal resistance increases. For the association of two new cells in parallel, SOH_C and SOH_2 are very different. The rated internal resistance of LIBs is usually given by the manufacturer, but in the case of these two cell models this value is not given. Thus, $R_{int,NEW}$ was considered to be the R_{int} measured in the 1st cycle. That value is considered to be the internal resistance at a SOH of 100%, which is not true, because in this case capacity shows to be at about 92% in the 1st cycle, which explains why there is such a difference between SOH_C and SOH_2. However, SOH_C and SOH_2 show to have a similar profile (SOH_2 having a more regular evolution), suggesting that if the rated $R_{int,NEW}$ value had been used for SOH_2 calculation, there could have been a correlation between both definitions.

Since for the used cell this approach does not correlate with SOH_C, it was intended to determine a value $R_{int,EOL}$ which, if used in SOH calculation, would allow approximating to SOH_C. $R_{int,EOL}$ is defined as $R_{int,EOL} = f \cdot R_{int,NEW}$. SOH based on resistance, calculated with this new $R_{int,EOL}$ value, is determined and defined as SOH_R. Using the tool *Solver* in *Microsoft Excel*, it was calculated the parameter f for the relationship $R_{int,EOL} = f \cdot R_{int,NEW}$, by establishing that the SOH_R of the last cycle should equal the SOH_C of the last cycle. This was done for all the tested cells, in order to understand what is the value f that best approximates SOH_C to SOH_R. $R_{int,NEW}$ was considered the value obtained for each test in the 1st cycle.

The factor f calculated for the new cell is 5.62, and for the used cell is 46.73. For the two new cells in parallel, f is 1.97 and for the two used cells in parallel f is 7.09.

Thus, SOH_R is calculated as follows:

$$SOH_{R,new\ cell} = \frac{5.62\,R_{int,NEW} - R_{int}}{5.62\,R_{int,NEW} - R_{int,NEW}} \times 100\% \quad (5)$$

$$SOH_{R,used\ cell} = \frac{46.73\,R_{int,NEW} - R_{int}}{46.73\,R_{int,NEW} - R_{int,NEW}} \times 100\% \quad (6)$$

$$SOH_{R,new\ cells} = \frac{1.97\,R_{int,NEW} - R_{int}}{1.97\,R_{int,NEW} - R_{int,NEW}} \times 100\% \quad (7)$$

$$SOH_{R,used\ cells} = \frac{7.09\,R_{int,NEW} - R_{int}}{7.09\,R_{int,NEW} - R_{int,NEW}} \times 100\% \quad (8)$$

The only disadvantage of calculating SOH based on internal resistance through EIS tests is that those values require an EEC to be obtained, even though other techniques could be used to readily obtain internal resistance values. Alternatively, the impedance modulus |Z| can be obtained by EIS without the need for an EEC. SOH was then calculated using |Z| (SOH_Z) instead of the internal resistance, to understand how this alternative correlates with SOH_C.

Using the *Solver* tool, the parameter f is obtained for the relationship $|Z|_{EOL} = f \cdot |Z|_{NEW}$, where |Z| is the impedance modulus at the lowest frequency. $|Z|_{NEW}$ was considered the value obtained for each test in the 1st cycle.

For the new cell f is 6.01 and for the used cell f is 20.30. For the parallel connected new cells, f is equal to 3.09, and for the used cells in parallel it is 3.21. SOH_Z is calculated as follows:

$$SOH_{Z,new\ cell} = \frac{6.01\,|Z|_{NEW} - |Z|}{6.01\,|Z|_{NEW} - |Z|_{NEW}} \times 100\% \quad (9)$$

$$SOH_{Z,used\ cell} = \frac{20.30\,|Z|_{NEW} - |Z|}{20.30\,|Z|_{NEW} - |Z|_{NEW}} \times 100\% \quad (10)$$

$$SOH_{Z,new\ cells\ //} = \frac{6\,|Z|_{NEW} - |Z|}{6\,|Z|_{NEW} - |Z|_{NEW}} \times 100\% \quad (11)$$

$$SOH_{Z,used\ cells\ //} = \frac{3.21\,|Z|_{NEW} - |Z|}{3.21\,|Z|_{NEW} - |Z|_{NEW}} \times 100\% \quad (12)$$

The main disadvantage of this approach is that |Z| of the cell as new is not currently given by the manufacturer.

SOH_C (SOH estimation based on capacity fade), SOH_2, SOH_R and SOH_Z were estimated for the different tests (Figures 11-14).

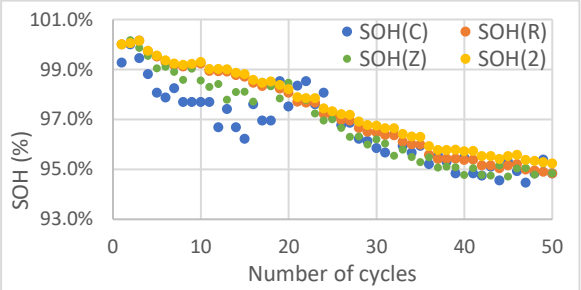

Figure 11: SOH of the new cell calculated based on capacity, SOH(C), internal resistance, SOH(R), impedance modulus at the lowest frequency, SOH(Z), and battery replacement criteria, SOH(2).

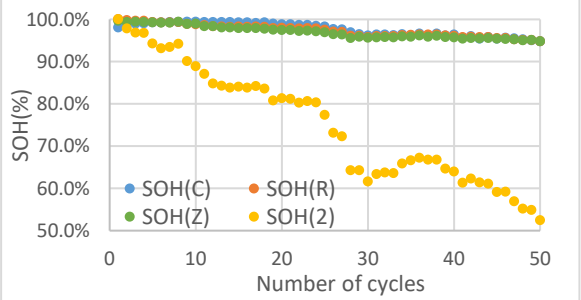

Figure 12: SOH of the used cell calculated based on capacity, SOH(C), internal resistance, SOH(R), impedance modulus at the lowest frequency, SOH(Z), and battery replacement criteria, SOH(2).

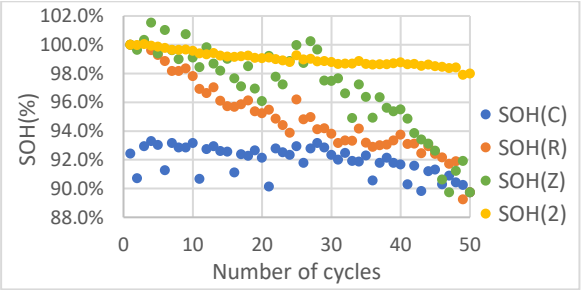

Figure 13: SOH of the two new cells in parallel, calculated based on capacity, SOH(C), internal resistance, SOH(R), impedance modulus at the lowest frequency, SOH(Z) and battery replacement criteria, SOH(2).

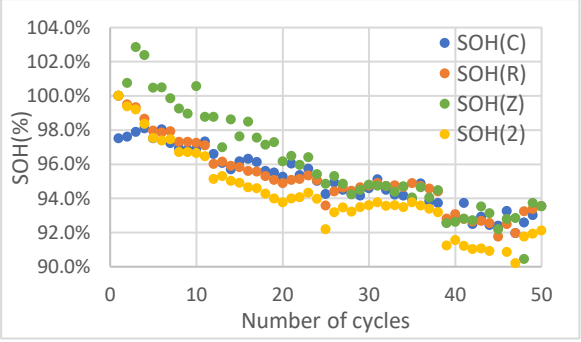

Figure 14: SOH of the two used cells in parallel, calculated based on capacity, SOH(C), internal resistance, SOH(R), impedance modulus at the lowest frequency, SOH(Z) and battery replacement criteria, SOH(2).

Fig. 11 reveals that the different approaches for SOH estimation of the new cell show a reasonable correlation with SOH_C. In fact, the factor f calculated for SOH_R and SOH_Z was found to be very close to 6, as in the theoretical approach. This suggests not only that SOH_C can be related to SOH determination based on internal resistance, but also that the resistance replacement criterion is in accordance with the capacity one, in this case. SOH_Z seems to be the approach which better approximates to SOH_C, by following the most accentuated capacity variations especially in the first half of the cycles, but for the second half of the cycles SOC_R is also a good approximation.

Regarding the used cell (Fig. 12), SOH_2 shows very different values compared to SOH_C, presenting a SOH_2 of 52% when the SOH_C remains at 95%, due to the fact that the cell's capacity decreased very little over 50 cycles, while R_{int} increased dramatically. In this case, SOH_R is the approach that mostly approximates to SOH_C. The determined f factors have a significant difference from the theoretical one (6), being 46.73 in $R_{int,EOL} = f \cdot R_{int,NEW}$ and 20.30 in $|Z|_{EOL} = f \cdot |Z|_{NEW}$.

For the two new cells in parallel, none of the approaches showed a good correlation with SOH estimation based on capacity, which is explained by the need to use the R_{int} and |Z| values of the 1st cycle as the $R_{int,NEW}$ and $|Z|_{NEW}$ values, since these are not given. Using these values results in a SOH of 100% in the 1st cycle, while the SOH based on capacity was 92.4% in the 1st cycle.

For the two used cells in parallel, SOH_R shows to be the best approximation to SOH_C, with a factor f of 7.09 in $R_{int,EOL} = f \cdot R_{int,NEW}$.

The results of the individual cells and of the two used cells in parallel show that there may be a correlation between SOH_C and SOH based on resistance or impedance. None of the batteries reached 80% of its rated capacity during the 50 cycles, therefore it would have been useful to study cell ageing over a higher number of cycles.

SOH_Z and SOH_R, based on impedance and internal resistance, respectively, revealed to be the best approximations to SOH_C for the new cell, while SOH_R based on resistance better approximates SOH_C for the used cell and for the two parallel-connected used cells. Since SOH_Z estimation is a more complicated approach because initial |Z| values are not given by the manufacturer, it is possible to see SOH_R as a

potential method to estimate SOH based on resistance and have a reasonable correlation with capacity variation.

According to the results, in order to have a correlation between SOH_R and SOH_C for both the new and the used cell, the factor f in $R_{int,EOL} = f \cdot R_{int,NEW}$ had to be significantly different for the two cases.While the factor f for the new cell is close to the one determined by battery replacement criteria, for the used cells this value is very different. Besides their ageing, these cells are of different models, therefore it is expected that they have different characteristics and behavior, and they might have different $R_{int,NEW}$ values. With this in mind, it would be interesting to verify at which extent the battery replacement criteria $R_{int} = 2R_{int,NEW}$ is adequate for all types of LIBs. Since different cells may have different compositions and characteristics, it would be reasonable to consider that they could have different replacement criteria and different $R_{int,EOL}$ in relationship with $R_{int,NEW}$. SOH_2 determination has a fixed f value of 6, implying that $R_{int,EOL} = f \cdot R_{int,NEW}$ is valid for all types of LIBs. While having this fixed value can be helpful in terms of generalization, and a reasonable approximation to most of the values that were determined in this work, finding the exact value for each cell model would allow for a more accurate SOH determination and a better correlation with SOH_C. In that case, if this type of study was previously made by the manufacturers, they could provide a value of $R_{int,EOL}$ in function of $R_{int,NEW}$, value at which the cell would be approximately reaching its end-of-life for both resistance and capacity thresholds.

The factor f in $R_{int,EOL} = f \cdot R_{int,NEW}$ was also found to be different in the cases of one individual used cell and two parallel-connected used cells. This factor is much larger for the individual cell ($f = 46.73$), which shows an extremely high increase of R_{int} during cycling, than for the association of used cells in parallel, where the factor f is 7.09, closer to the theoretical value. It is unclear if this high increase of R_{int} for the individual is solely related to extreme power fade of that specific cell or if any experimental errors may have affected the measurements. Therefore, studying the hypothesis of $R_{int,EOL} = f \cdot R_{int,NEW}$ having a different f value for each cell type would require performing cycling tests to a larger number of cells of the module to verify if overall they show similar f values. Nevertheless, the f factor calculated for the used parallel-connected cells was different than 6, which also suggests that by having a $R_{int,EOL}$ specific for each cell model, a better correlation between SOH_C and SOH determination based on internal resistance could be achieved.

Therefore, an underpinned study on this possible correlation requires a much larger sample of cells to be studied, of different characteristics, as well as a larger number of cycles.

6. Conclusions

This work allowed contributing to a better understanding of the ageing mechanisms governing lithium-ion cells by means of capacity and impedance analysis through charge-discharge tests and EIS. EIS tests revealed that overall impedance increases with cycling, but this evolution is not linear, and some decreases can occur. Furthermore, some of these changes might only be perceived after a large number of cycles, meaning that 50 cycles are insufficient for a complete ageing study and longer tests should be done.

It was verified that R_{int} is indeed the parameter that contributes the most to the impedance modulus, both for the individual and parallel-connected cells. In addition, unlike R_{SEI}, which does not show significant variation over 50 cycles, and R_{CT} and W_o, which vary mostly with SOC, R_{int} changes mostly with the number of cycles, being therefore considered a good indicator of cell ageing to be used in SOH determination.

SOH was estimated based on the condition that a battery should be replaced when its internal resistance doubles, and assuming that in that moment the SOH is 80%. The R_{int} value when the battery's SOH is 0% was determined as $R_{int,EOL} = 6\ R_{int,NEW}$. This SOH determination method was found to approximate reasonably to SOH_C for the individual new cell and for the parallel-connected new cells and used cells, but not for the individual used cell. Thus, a factor f in the relationship $R_{int,EOL} = f \cdot R_{int,NEW}$ that better approximates to SOH_C was determined and SOH_R was calculated using that factor for each test. The same was done by using the impedance modulus |Z| at the lowest frequency instead of R_{int} in order to have an alternative that does not require an EEC. The factor f was calculated and SOH_Z with that factor f was determined. SOH_R revealed to be the most approximate estimation approach to SOH_C, and it implies that different cell types would have different internal resistance values corresponding to the moment when the cell dies, $R_{int,EOL}$, as function of the initial internal resistance of the cell, $R_{int,NEW}$, which is reasonable to consider since different cell types can have different initial resistance values and ageing behavior.

In any case, it is important to emphasize that extended tests would be necessary to have a complete analysis of capacity and impedance evolution with cycling, as well as to study the relationship between R_{int} increase and capacity fade, and to conclude on a suitable SOH determination method based on resistance.

6.1. Future Work

As a continuation of this work, it becomes important to extend the charge-discharge and EIS tests to a larger number of cells, in order to verify the results obtained for a single cell and to identify possible errors associated with experimental conditions. Additionally, it would also be useful to subject the cells to a greater number of cycles, or even cycling them until failure, to obtain more information about the evolution of capacity and impedance of the cell over its entire life. This would also allow determining R_{int} of the cell at the time of failure, which could be useful in ascertaining the feasibility of the presented approaches for impedance-based SOH calculation. Moreover, in order to study the applicability of impedance-based SOH for diagnostics of complete electric vehicle battery modules or cell stacks, it would be important to extend these studies to multiple cells connected both in series and in parallel.

References

(1) Dunn, B.; Kamath, H.; Tarascon, J.-M. Electrical Energy Storage for the Grid: A Battery of Choices. *Science (1979)* **2011**, *334*, 928–935. https://doi.org/10.1126/science.1212741.

(2) Ellingsen, L. A. W.; Majeau-Bettez, G.; Singh, B.; Srivastava, A. K.; Valøen, L. O.; Strømman, A. H. Life Cycle Assessment of a Lithium-Ion Battery Vehicle Pack. *J Ind Ecol* **2014**, *18* (1), 113–124. https://doi.org/10.1111/jiec.12072.

(3) Energy Agency, I. *Global EV Outlook 2021: Accelerating Ambitions despite the Pandemic*; 2021. https://www.iea.org/reports/global-ev-outlook-2021/ (accessed Sep. 16, 2022).

(4) Saha, B.; Goebel, K. *Modeling Li-Ion Battery Capacity Depletion in a Particle Filtering Framework*; 2009.

(5) Xia, W.; Mahmood, A.; Zou, R.; Xu, Q. Metal-Organic Frameworks and Their Derived Nanostructures for Electrochemical Energy Storage and Conversion. *Energy and Environmental Science*. Royal Society of Chemistry July 1, 2015, pp 1837–1866. https://doi.org/10.1039/c5ee00762c.

(6) Ozawa, Kazunori. *Lithium Ion Rechargeable Batteries*; Wiley-VCH, 2009.

(7) Barai, A.; Uddin, K.; Dubarry, M.; Somerville, L.; McGordon, A.; Jennings, P.; Bloom, I. A Comparison of Methodologies for the Non-Invasive Characterisation of Commercial Li-Ion Cells. *Progress in Energy and Combustion Science*. Elsevier Ltd May 1, 2019, pp 1–31. https://doi.org/10.1016/j.pecs.2019.01.001.

(8) Kasnatscheew, J.; Wagner, R.; Winter, M.; Cekic-Laskovic, I. Interfaces and Materials in Lithium Ion Batteries: Challenges for Theoretical Electrochemistry. *Topics in Current Chemistry*. Springer International Publishing June 1, 2018. https://doi.org/10.1007/s41061-018-0196-1.

(9) Gamry Instruments. *Testing Lithium-Ion Batteries*. Application note. https://www.gamry.com/application-notes/battery-research/testing-lithium-ion-batteries/ (accessed Apr. 2, 2022)

(10) Omar, N.; Daowd, M.; van den Bossche, P.; Hegazy, O.; Smekens, J.; Coosemans, T.; van Mierlo, J. Rechargeable Energy Storage Systems for Plug-in Hybrid Electric Vehicles-Assessment of Electrical Characteristics. *Energies (Basel)* **2012**, *5* (8), 2952–2988. https://doi.org/10.3390/en5082952.

(11) Zappen, H.; Fuchs, G.; Gitis, A.; Sauer, D. U. In-Operando Impedance Spectroscopy and Ultrasonic Measurements during High-Temperature Abuse Experiments on Lithium-Ion Batteries. *Batteries* **2020**, *6* (2). https://doi.org/10.3390/batteries6020025.

(12) *Lithium-Lon Batteries Solid-Electrolyte Interphase*. Imperial College Press, 2004.

(13) Pastor-Fernández, C.; Uddin, K.; Chouchelamane, G. H.; Widanage, W. D.; Marco, J. A Comparison between Electrochemical Impedance Spectroscopy and Incremental Capacity-Differential Voltage as Li-Ion Diagnostic Techniques to Identify and Quantify the Effects of Degradation Modes within Battery Management Systems. *J Power Sources* **2017**, *360*, 301–318. https://doi.org/10.1016/j.jpowsour.2017.03.042.

(14) Iurilli, P.; Brivio, C.; Wood, V. On the Use of Electrochemical Impedance Spectroscopy to Characterize and Model the Aging Phenomena of Lithium-Ion Batteries: A Critical Review. *Journal of Power Sources*. Elsevier B.V. September 1, 2021. https://doi.org/10.1016/j.jpowsour.2021.229860.

(15) Raj, T.; Wang, A. A.; Monroe, C. W.; Howey, D. A. Investigation of Path-Dependent Degradation in Lithium-Ion Batteries. *Batter Supercaps* **2020**, *3* (12), 1377–1385. https://doi.org/10.1002/batt.202000160.

(16) Dong, G.; Wei, J. A Physics-Based Aging Model for Lithium-Ion Battery with Coupled Chemical/Mechanical Degradation Mechanisms. *Electrochim Acta* **2021**, *395*. https://doi.org/10.1016/j.electacta.2021.139133.

(17) Preger, Y.; Barkholtz, H. M.; Fresquez, A.; Campbell, D. L.; Juba, B. W.; Romàn-Kustas, J.; Ferreira, S. R.; Chalamala, B. Degradation of Commercial Lithium-Ion Cells as a Function of Chemistry and Cycling Conditions. *J Electrochem Soc* **2020**, *167* (12), 120532. https://doi.org/10.1149/1945-7111/abae37.

(18) Hu, X.; Feng, F.; Liu, K.; Zhang, L.; Xie, J.; Liu, B. State Estimation for Advanced Battery Management: Key Challenges and Future Trends. *Renewable and Sustainable Energy Reviews*. Elsevier Ltd October 1, 2019. https://doi.org/10.1016/j.rser.2019.109334.

(19) Murnane, M.; Ghazel, A. *A Closer Look at State of Charge (SOC) and State of Health (SOH) Estimation Techniques for Batteries*.

(20) Ungurean, L.; Cârstoiu, G.; Micea, M. v.; Groza, V. Battery State of Health Estimation: A Structured Review of Models, Methods and Commercial Devices. *International Journal of Energy Research*. John Wiley and Sons Ltd February 1, 2017, pp 151–181. https://doi.org/10.1002/er.3598.

(21) Choi, W.; Shin, H. C.; Kim, J. M.; Choi, J. Y.; Yoon, W. S. Modeling and Applications of Electrochemical Impedance Spectroscopy (Eis) for Lithium-Ion Batteries. *Journal of Electrochemical Science and Technology*. Korean Electrochemical Society February 1, 2020, pp 1–13. https://doi.org/10.33961/jecst.2019.00528.

(22) Dai, H.; Jiang, B.; Wei, X. Impedance Characterization and Modeling of Lithium-Ion Batteries Considering the Internal Temperature Gradient. *Energies (Basel)* **2018**, *11* (1). https://doi.org/10.3390/en11010220.

(23) Krause, F. C.; Ruiz, J. P.; Jones, S. C.; Brandon, E. J.; Darcy, E. C.; Iannello, C. J.; Bugga, R. v. Performance of Commercial Li-Ion Cells for Future NASA Missions and Aerospace Applications. *J Electrochem Soc* **2021**, *168* (4), 040504. https://doi.org/10.1149/1945-7111/abf05f.